Journal of
Materials Chemistry C

Accepted Manuscript

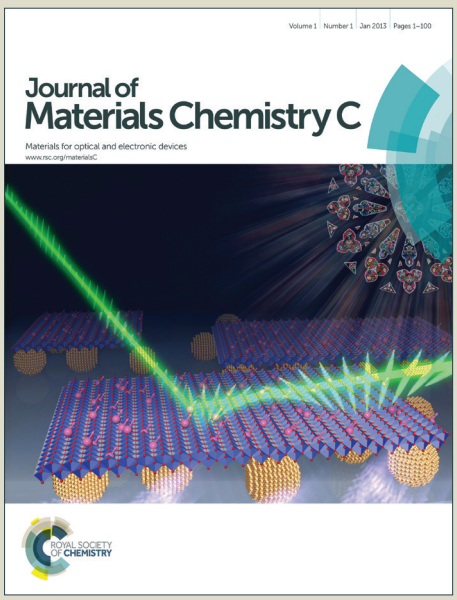

ROYAL SOCIETY OF CHEMISTRY

www.rsc.org/materialsC

Fluorescent Au-Ag Alloy Cluster Synthesis and SERS Applications

Bipattaran Paramanik and Amitava Patra*

Department of Materials Science, Indian Association for the Cultivation of Science, Kolkata 700 032, India

*Author to whom correspondence should be addressed; electronic mail: msap@iacs.res.in Phone: (91)-33-2473-4971, Fax: (91)-33-2473-2805

Abstract

Fluorescent metal nanoclusters have recently emerged as a new class of functional materials because of their potential applications in photocatalysis, water splitting, light harvesting or others. Here, we have demonstrated the synthesis of highly blue luminescent AuAg bimetallic alloy cluster by simple one pot bottom up method. Transmission electron microscopy (TEM), X-ray photoelectron spectroscopy (XPS), and photoluminescence (PL) have been used to characterize the alloy clusters. A dramatic blue shifting of PL peak (from 608 nm to 444 nm) reveal a drastic change of electronic transition in presence of Ag^+, due to formation of new cluster. We have been given emphasis on the influence of the capping ligand, pH or metal ions on the cluster formation and their stability. Based on the controlled experiments and galvanic theory, anti-galvanic reaction mechanism has been proposed for the formation of bimetallic AuAg alloy cluster. Surface Enhanced Raman Scattering (SERS) intensity is found to be increased in presence of AuAg alloy cluster and the enhancement factor (EF) found to be 1.44 x 10^6 for alloy AuAg nanocluster.

Introduction

Ultrasmall noble metal nanoparticles are known as metal clusters having typical size in between metal atom and metal nanopaticle (NP). [1-3] Unlike NP, the density of the state in nanoclusters is not strong enough to show shape and size dependent surface plasmon resonance (SPR).[4-6] Rather, it exhibits molecule likes d-sp, sp-sp distinct transition and intense fluorescence due to quantum confinement, which is a unique property of nanoclusters.[7, 8] The photoluminescence wavelength of metal nanocluster (NC) can be tuned form near-infrared (NIR) to ultraviolet (UV) either by varying the number of core atoms or by changing the protecting ligand of the cluster.[9-12] It is reported that Ag_7 cluster (silver cluster composed of 7 atoms of Ag) exhibits intense blue luminescent however Ag_8 cluster exhibits NIR-red emission.[13] Jin and his coworkers[10] have demonstrated that Au_{25} cluster exhibits different photophysical properties depending on ligand-to-metal charge transfer (LMCT) or ligand-to metal-metal charge transfer (LMMCT). The stability and solubility of noble metal NCs are governed by the capping ligands and the commonly used capping ligands contain N, O, P and S atom.[2, 11, 14-16] Thiols are often used as capping ligand for Au, Ag, Cu even Pt NC.[12, 15, 17] Thioalcohols, thioacids and sulfur containing amino acids or peptides are widely used for water soluble metal cluster synthesis.[17, 18] Multi-thiol based ligand is also used for the synthesis of stable NIR emissive AuNC.[7] Mattoussi et al.[19, 20] have elaborated the influence of zwitterionic anchor on the photophysics (QY, lifetime etc.) and stability of AuNC or AgNC. Generally, two methods are being used for preparing metal clusters, either by one step bottom up approach or by two step top down method. [7, 21-23] Yao and coworkers[24] have reported the synthesis of Au_{18} and Au_{15} by changing the pH of the solution only, without changing precursor and capping ligand.

The potential applications of such noble metal cluster are found to be in living cell imaging, sensing of toxic metal ions or biomolecules by using PL signal of the NC.[23, 25-31] Nevertheless, hybrid and composite of nanoclusters are found to be potential candidates in photocatalysis, water splitting, light harvesting, CO oxidation, alcohol oxidation, sensing or other multimodal applications.[11, 32-34] Unlike pure AgNC or AuNC, AuAg alloy NC possess higher stability owing to the presence of nobler Au and high QY due to the Ag.[35] Two step methods for synthesis of bimetallic cluster have been reported by Xie and his co-workers.[36] In this method, Ag^+ is added with AuNC, where Ag^+ helps to bridge Au^+-thiolate motifs on the AuNC surface.

Thus, AuNC is surrounded by the large network of Au^+/Ag^+-thiolate, produces highly luminescent AuAg alloy cluster.[36]

In this report, we have synthesized highly efficient blue luminescent bimetallic AuAg alloy cluster by simple one pot bottom up method. We, also provide an alternative top down method for the synthesis of same bimetallic cluster. Several characterization methods (TEM, XPS, matrix-assisted laser desorption ionization-time of flight and PL) are being used to characterize these alloy clusters. A mechanism for the formation of bimetallic alloy cluster has been proposed. Finally, surface enhanced Raman scattering (SERS) enhancement of methlyene blue (MB) in presence of bimetallic alloy cluster is reported.

Experimental Section

One pot synthesis of gold nanocluster (AuNC) and gold-silver alloy nanocluster (AuAgNC)

The synthesis of Au nanocluster[21] by using thiol induced reduction of Au^{3+} to Au^0 is given in supporting information (ESI). For synthesis of gold-silver alloy nanoclusters, different amounts (5 μL to 160 μL) of 1 wt % Ag^+ were mixed with 80 μL of 1 wt % Au^{3+} and these were kept for incubation at dark without stirring for 5-6 hours. Finally purification was done by centrifugation followed by dialysis. Solution having highest blue fluorescent intensity upon excitation at 375 nm was stored for further experiment.

Etching directed Synthesis of gold-silver alloy nanocluster (AuAgNC)

For etching directed synthesis of 2.5 mL of diluted AuNP[23] (see ESI) solution was mixed with 60 μL of 1 wt % Ag^+ and pH of the solution was adjusted by 0.5 mL of 50 mM borax. To this solution, 1.25 mL of 40 mM MUA in ethanol was added. Then, the mixture was etched at dark for 72 hours. Sample was centrifuged at 10000 rpm for 10 min to remove the bigger AuNPs and supernatant was dialyzed for 6 hours. Highly blue luminescent alloy clusters were stored in at 4^0C.

Characterization

Room-temperature optical absorption spectra were recorded by UV-Vis spectrophotometer (Shimadzu) using a cuvette of 1 cm path length. The emission spectra of all samples were obtained with FluoroMax-P (HORIBA Jobin Yvon) luminescence spectrophotometer. Quantum yield (QY) of the alloy NC and AuNC were measured using quinine sulfate and rhodamine 6G as reference dye, respectively. The transmission electron microscopy (TEM) image and the energy dispersive spectroscopy (EDS) were taken using JEOL-JEM-2100F transmission electron

microscope. Mapping of AuAgNC was performed by high-angle annular dark-field imaging (HAADF) in scanning transmission electron microscope (STEM) mode of the same TEM instrument. The size of the NCs are also measured by matrix-assisted laser desorption ionization-time of flight (MALDI-TOF) mass spectrometry on Bruker Daltonics Autoflex II TOF/TOF system. A pulse laser of 337 nm and saturated DHB solution was selected as matrix for MALDI-TOF measurement. Raman spectra of the films were recorded by exciting the sample with an Ar^+ ion laser source of 1.0 mW power at the sample with T64000 model made of Horiba Jobin Yvon.

Results and Discussion

11-mercaptoundecanoic acid (MUA) is chosen as a capping ligand for synthesis of nanocluster (NC). MUA also acts as mild reducing agent[21] for the conversion of Au^{3+} to Au^0. Figure 1A (red curve) depicts a strong absorption peak at 390 nm along with two weak absorption humps at 280 nm, and 320 nm which are due to the d-sp and sp-sp transition of AuNC.[7, 34] No absorption band due to surface plasmon resonance (SPR) at 520 nm,[37, 38] is observed which confirms no formation of Au NP in the present experimental conditions.[1] The photoluminescence spectrum (red curve of Fig. 1B) demonstrates a strong orange-red emission at 608 nm for as synthesized AuNC. The PL intensity of the luminescent AuNC increases with increasing Au: S ratio and then it decreases. In the present study, the highest fluorescent intensity of AuNC, having quantum yield (QY) 2.4% is obtained at 1.0: 5.0 of ratio Au: S. Thus, we choose 1.0: 5.0 ratio of Au: S for bimetallic cluster synthesis. To achieve bimetallic cluster, different amounts of Ag^+ are directly added to the mixture of Au^{3+} and MUA. The absorption peak at 390 nm of AuNC (Fig. 1A, blue curve) is shifted to 334 nm and the orange-red emission (608 nm) of AuNC is blue shifted to 444 nm (almost 166 nm blue shift, shown in Fig. 1B) at a ratio of Ag: Au (1.0: 1.75). The dramatic blue shifting of absorption and PL peak reveal a drastic change of electronic transition in presence of Ag^+, due to formation of new cluster. In such alloy cluster, Xie et al.[36] have proposed this strong fluorescence of bimetallic clusters is mainly due to Au(I)/Ag(I) complex formation. The highest quantum yield (QY) is found to be 3.0 % for 1.0: 1.75 ratio of Ag: Au. Digital photographs (Fig. S1, ESI) also support the change of brightness, color tunability of cluster with changing Ag: Au. It is interesting to note that the absorbance peak at 334 increases with increasing incubation time (50 min to 5 hours) for 1.0: 1.75 ratio of Ag: Au (Fig. 2A). The PL intensity (at 444 nm) increases significantly after 4hrs incubation time (Fig. 2B) due to completion of cluster formation.

It is clearly seen from TEM image (Fig. 3A) that the formation of ultrasmall monodispersed Au NC with an average particles size is 1.6 ± 0.5 nm. The TEM image of AuAg bimetallic cluster (Fig. 3B) demonstrates the uniform particle size distribution and the average diameter of the bimetallic clusters is 1.7± 0.5 nm. In normal TEM resolution, it is not possible to differentiate AuNC and AuAg bimetallic nanocluster. Therefore, HAADF-STEM technique has been used for elemental mapping of this cluster. The rectangular box in the Fig. 3C shows the area which is taken for elemental mapping (Fig. 3D-F) of S, Au and Ag, respectively. Analysis confirms the presence of both Au and Ag in AuAg bimetallic nanocluster. Again, the distinct peaks of Au and Ag from EDS study also confirm the formation of bimetallic cluster (Fig. S2). MALDI-TOF mass is being used to find the mass or composition of NC. Fig. S3 shows the MALDI-TOF spectrum for the Au NC. The peak at m/z ~ 6427 is probably due to the AuNC, having molecular formula $Au_{16}MUA_{15}$. The peaks at m/z ~6011, 5596 or others are coming from $Au_{16}MUA_{15}$ unit by the dissociation of Au_1MUA_1, Au_2MUA_2 or Au_xMUA_x fragments. In case of AuAg alloy NC, a broad hump at m/z ~3300 to 5000 is observed (Fig. S4), indicating AuAg alloy formation with different molecular formula which is consistent with previous result.[36]

To well characterize this bimetallic cluster, XPS study is being performed. Figure 4A shows the binding energy of gold $4f_{7/2}$ and $4f_{5/2}$ are 85.03 eV and 88.07 eV, respectively and the intensity ratio of $4f_{7/2}$: $4f_{5/2}$ is 1.23: 1.0. The shifting of the peak ($4f_{7/2}$) with respect to bulk Au^0 (84.0 eV) and Au^{1+} (86.0 eV) confirms the AuNC formation where Au is neither in Au^0 nor in Au^{1+} state.[21] The co-existence of Au^0 and Au^{1+} state is also a special characteristic of AuNC.[39] In the de-convoluted XPS curve (Fig. 4B); the binding energy of S $2p_{3/2}$ is 162.42 eV which is consistence with the previous report.[40] The additional peak at 163.78 eV is due to disulfide formation by MUA. As no external reducing agent is used, some of the thiols are converted to dithiols and Au^{3+} are reduced to Au^0/Au^+. On the other hand, the peak intensity of Au $4f_{7/2}$ reduces with respect to $4f_{5/2}$ in bimetallic cluster, as silver is present. The intensity ratio of $4f_{7/2}$:$4f_{5/2}$ is 1.23: 1.0 for pure AuNC and it decreases to 0.17: 1.0 in presence of silver, confirming the bimetallic cluster which is different from the pure AuNC.[39] Like pure AuNC (Fig. 4A), bimetallic cluster also possess Au^{+1} state on the surface, which have great potential to show metallophilic interaction.[41] Therefore, we believe the influence of metallophilic (d^{10}-d^{10} of Au^+ and/ Ag^+) interaction as reflected from XPS spectra, which is responsible for the enhancement of peak (Fig. 4C) intensity ratio of $4f_{7/2}$: $4f_{5/2}$ in presence of Ag^+. The binding energy for bulk silver

and its zero state are 368.2 and 374.2 eV for Ag $3d_{5/2}$ and Ag $3d_{3/2}$ respectively.[42] In the as synthesized bimetallic cluster, the binding of Ag $3d_{5/2}$ and Ag $3d_{3/2}$ are at around 367.54 eV and 373.3 eV, respectively (Fig. 4D), which confirms the zero state of Ag. Thus, Ag influences the alloy NC formation either by bridging the Au-S motifs or metallophilic interaction.

The control experiments have been performed to understand the influence of the capping ligand, pH or metal ions on the cluster. The stability of the cluster and alternative way of synthesis of same bimetallic cluster has also been investigated. For any cluster synthesis, the crucial steps are ligand-metal complex formation followed by reductive decomposition of the complex. It is noted that no cluster (Fig. 5A) formation is observed in presence of GSH (glutathione) or CYS (L-cysteine) because Au^+-GSH or Au^+-CYS complex are extremely soluble in water. In the present study, ethanol is added to aqueous solution of MUA to enhance the solubility. MUA is negatively charged (as pH≈ 9 in our experiment), it forms strong complex with Au^+/Ag^+ which will neutralize the charge. The aggregates of Au^+/Ag^+-MUA produces highly fluorescent AuNC or AuAg bimetallic alloy clusters in alkaline medium.[36] On the other hand, Cu^{2+} or Pt^{4+} does not form luminescent cluster in presence of MUA even in alkaline medium (Fig. 5B). It is interesting to note that the AuAg alloy clusters are stable in presence of both oxidizing (H_2O_2) and reducing ($NaBH_4$) agents. However, the cluster structure breaks down in addition of large excess of $NaBH_4$ and H_2O_2 as evident from PL study (Fig. 5C and D).

To find any alternative method for synthesis of bimetallic cluster, core-etching technique is being used. The incubation of MUA with a mixture of AuNP and Ag^+ for 6 hours produces orange-red emitting AuNC. The blue emission at 444 nm is observed (Fig. S5) if incubation time is increased for 3 days, which is similar to as synthesized one pot method. This phenomenon elucidates that the orange-red emitting AuNC may be formed as an intermediate before bimetallic blue emitting AuAgNC formation. Then, the intermediate AuNC in-situ is converted to AuAgNC in presence of Ag^+ and excess MUA. It is clearly seen from TEM images (Fig. 6A-D) that the size of the AuNP drastically reduces after etching with MUA. The bimetallic NC is synthesized by a top down (core etching) method, having average particle size of 1.7± 0.5 nm, which matches well with the bimetallic NC synthesized by one pot method. Hence, core etching is found to be an alternative top down way for size selective synthesis of bimetallic NC. Although, one pot method is definitely a less time taken superior approach, compared to top down method. In a control experiment, no blue emitting cluster formation occurs even when Ag^+

is added with green emitting AuNC. On the other hand, if AgNP is added with the mixture of Au^{3+}-MUA and incubated for 2 days, the solution color changes from brown to black. The supernatant exhibits intense blue luminescent similar to bimetallic cluster (Fig. S6).

Based on experimental results, the following observations are made: (1) orange-red emitting (emission at 608 nm) AuNC is observed when Au^{3+} incubated with MUA. (2) No fluorescent NC is observed when Ag^{+} incubated with MUA and AgCl precipitation is obtained on addition of KCl to this solution. (3) In one pot method, incubation of the mixture of Au^{3+} and Ag^{+} with MUA for 6 hours produces blue emitting (444 nm) bimetallic AuAgNC and addition of KCl to this solution does not produce any AgCl precipitation. (4) Etching of AuNP with Ag^{+} and MUA for 6 hours produces orange-red emission. Three days incubation produces blue emitting bimetallic AuAgNC, like one pot method. (5) Addition followed by incubation for 2 days of AgNP in the mixture of Au^{3+} and MUA produces blue luminescent bimetallic AuAgNC. A schematic diagram (Scheme 1) is given based on the above discussion.

The standard electrode potential (E^0) of different systems are given below;

$$[AuCl_4]^- + 3e \rightleftharpoons Au^0(s) \qquad [E^0 = 0.99\ V] \qquad (1)$$

$$[AuCl_2]^- + e \rightleftharpoons Au^0(s) \qquad [E^0 = 1.51\ V] \qquad (2)$$

$$Ag^+ + e \rightleftharpoons Ag^0(s) \qquad [E^0 = 0.799\ V] \qquad (3)$$

Thus electrochemistry suggests the following reaction is favorable according to classical galvanic theory: $Au^{3+}/ Au^{+1} + Ag^0 (s) \rightarrow Ag^+ + Au^0 (s)$ and the reverse reaction should not be happened.[42] However, the XPS and EDX confirms that both Au^0 and Ag^0 are present in our bimetallic nanocluster, though initially Au^{3+} and Ag^+ are incubated in presence of reducing and capping agent MUA. Furthermore, addition of KCl to this solution does not produce precipitation of AgCl, which confirms the presence of 0 state of silver, not in +1 state. It indicates that Ag^+ is converted to Ag^0 in presence of Au^0 or Au^+-MUA complex. Thus, the conversion of Ag^+ to Ag^0 in presence of Au^0 or Au^+-MUA complex violates the classical galvanic rule. It reveals that anti-galvanic reaction occurs in presence of Au cluster in one pot synthesis which is unprecedented. In top down method, excess thiol dissolves the gold atom from AuNP surface and form Au^+-S complex.[23] This Au^0-S or Au^+-S makes the unfavorable reaction spontaneous (reduction of Ag^+ to Ag).[43] Thus, silver helps to link the Au^0-S and Au^{+1}-S motifs

via strong metallophilic (d^{10}-d^{10}) interaction. In fact, the actual mechanism of cluster formation is still in debate. Based on our experimental findings and the previous reports[21, 22, 42] the plausible reactions for bimetallic cluster formations are:

$$Au^{3+} + MUA\text{-}S \rightarrow Au^{0}\text{-}S\text{-}MUA + Au^{+}\text{-}S\text{-}MUA + MUA\text{-}S\text{-}S\text{-}MUA \quad (4)$$

$$Au^{0}\text{-}MUA + Au^{+}\text{-}S\text{-}MUA + Ag^{+} \rightarrow AuAgMUA \quad (5)$$

On the other hand, when AgNP (Ag^0) is added with the mixture of Au^{3+} and excess MUA, very quickly the classical galvanic reaction takes place i.e. $Ag^0 + Au^{3+} \rightarrow Ag^+ + Au^0$. Then, the small atoms or clusters of Au^0 interacts with MUA which again in-situ reduce the Ag^+ by anti-galvanic reaction and followed by metallophilic interaction produces the bimetallic AuAgNC. Thus, strong anti-galvanic reaction prior to the metallophilic interactions is the key factor for the formation of alloy cluster.

The bimetallic alloy nanocluster is further investigated for the surface Raman enhancement study. Figure 7 shows the Raman spectra of the methylene blue (MB) molecules in the presence and absence of cluster. It is known that surface areas of NCs are much higher than the NPs or bulk system. Subsequently, the capability of dye adsorption on the NC surface is much higher than the NP surface which facilitates the SERS enhancement. The most intense peak at 1618 cm^{-1} is due to C-C stretching of the ring of MB. On the other hand, peak at 1395 cm^{-1}, 1450 cm^{-1} and 445 cm^{-1} are assigned for the Raman spectra of MB due to symmetric, asymmetric starching and bending of the C-N-C skeleton, respectively.[44] No significant Raman signal at 1618 cm^{-1} or 445 cm^{-1} are observed when AuNC is mixed with a nonfluorescent MB dye. However, in presence of AuAg bimetallic alloy cluster, a significant SERS enhancement (calculated enhancement factor is 1.44 x 10^6) of MB is observed (Fig. 7) with respect to pure MB. The enhancement factor (EF) is calculated by the following well established expression[45]

$$EF = (I_{SERS}/ N_{ads})/(I_{bulk}/ N_{bulk}) \quad (6)$$

Where I_{SERS} represents the intensity of a vibrational mode in the surface enhanced spectrum, I_{bulk} is the intensity of the Raman spectrum of same vibrational mode in, N_{ads} is the number of molecules adsorbed on the SERS-active substrate, and N_{bulk} is the number of molecules sampled on the bulk. In the present case, dye adsorption on the alloy surface, interaction with local electromagnetic field which makes alloy a promising SERS enhancer species than pure AuNC.[46, 47]

Conclusion

Highly blue luminescent AuAg alloy nanoclusters have been synthesized using one pot bottom up approach without using external reducing agent. Mercaptoundecanoic acid (MUA) is being used for both capping and reducing agent. We also provide an alternative top down method for the synthesis of same AuAg NC. An interesting anti-galvanic reaction is proposed to explain the alloy cluster formation which unprecedented. Numbers of controlled experiments confirm that Ag present at 0 oxidation state and Au present at 0 along with +1 oxidation state. Analysis suggests that both top down and bottom up approaches follow anti-galvanic reaction for alloy cluster formation. The SERS properties of alloy bimetallic cluster exhibit significant enhancement of Raman signal. The enhancement factor is found to be 1.44x 10^6 in presence of MB dye. Thus, we believe this alloy AuAg NC would be very promising for emission tuning and to detect the hazardous dye by SERS enhancement.

Acknowledgements

"DAE-SRC Outstanding Investigator Award" and SERB, DST are gratefully acknowledged for financial support. BP thanks CSIR for awarding fellowship.

† Electronic Supplementary Information (ESI) available: [Experimental details, digital photographs of the cluster, EDS of bimetallic cluster, MALDI-TOF spectrum of clusters, PL spectra of bimetallic cluster by top down method and time dependent PL spectra of the mixture of AgNP and Au^{3+}]. See DOI: 10.1039/b000000x/

References

1. J. Zheng, C. Zhang and R. M. Dickson, *Phys. Rev. Lett.*, 2004, 93, 077402-1.
2. R. Jin, *Nanoscale*, 2010, 2, 343.
3. Y. Negishi, K. Nobusada and T. Tsukuda, *J. Am. Chem. Soc.*, 2005, 127, 5261.
4. K. L. Kelly, E. Coronado, L. L. Zhao and G. C. Schatz, *J. Phys. Chem. B*, 2002, 107, 668.
5. K.-S. Lee and M. A. El-Sayed, *J. Phys. Chem. B*, 2006, 110, 19220.
6. A. Arbouet, C. Voisin, D. Christofilos, P. Langot, N. Del Fatti, F. Vallee, J. Lerme, G. Celep, E. Cottancin, M. Gaudry, M. Pellarin, M. Broyer, M. Maillard, M. P. Pileni and M. Treguer, *Phys. Rev. Lett.*, 2003, 90, 177401-1.
7. L. Shang, S. Brandholt, F. Stockmar, V. Trouillet, M. Bruns and G. U. Nienhaus, *Small*, 2012, 8, 661.
8. M. Zhu, C. M. Aikens, F. J. Hollander, G. C. Schatz and R. Jin, *J. Am. Chem. Soc.*, 2008, 130, 5883.
9. J. Zheng, P. R. Nicovich and R. M. Dickson, *Ann. Rev. Phys. Chem.*, 2007, 58, 409.
10. Z. Wu and R. Jin, *Nano Lett.*, 2010, 10, 2568.
11. G. Li and R. Jin, *Acc. Chem. Res.*, 2013, 46, 1749.
12. D. M. Chevrier, M. A. MacDonald, A. Chatt, P. Zhang, Z. Wu and R. Jin, *J. Phys. Chem. C*, 2012, 116, 25137.
13. T. Udaya Bhaskara Rao and T. Pradeep, *Angew. Chem. Int. Ed.*, 2010, 49, 3925.
14. H. Qian, M. Zhu, Z. Wu and R. Jin, *Acc. Chem. Res.*, 2012, 45, 1470.
15. J. Yu, S. A. Patel and R. M. Dickson, *Angew. Chem. Int. Ed.*, 2007, 46, 2028.
16. J. Zheng, J. T. Petty and R. M. Dickson, *J. Am. Chem. Soc.*, 2003, 125, 7780.
17. X. Yuan, Z. Luuuo, Q. Zhang, X. Zhang, Y. Zheng, J. Y. Lee and J. Xie, *ACS Nano*, 2011, 5, 8800.
18. L.-Y. Chen, C.-M. Ou, W.-Y. Chen, C.-C. Huang and H.-T. Chang, *ACS Appl. Mater. Interfaces*, 2013, 5, 4383.
19. F. Aldeek, M. A. H. Muhammed, G. Palui, N. Zhan and H. Mattoussi, *ACS Nano*, 2013, 7, 2509.
20. M. A. H. Muhammed, F. Aldeek, G. Palui, L. Trapiella-Alfonso and H. Mattoussi, *ACS Nano*, 2012, 6, 8950.
21. J. Sun, J. Zhang and Y. Jin, *J. Mater. Chem. C*, 2013, 1, 138.

22. Z. Luo, X. Yuan, Y. Yu, Q. Zhang, D. T. Leong, J. Y. Lee and J. Xie, *J. Am. Chem. Soc.*, 2012, 134, 16662.
23. C.-C. Huang, Z. Yang, K.-H. Lee and H.-T. Chang, *Angew. Chem. Int. Ed.*, 2007, 46, 6824.
24. Q. Yao, Y. Yu, X. Yuan, Y. Yu, J. Xie and J. Y. Lee, *Small*, 2013, 9, 2696.
25. X. Yuan, Z. Luo, Y. Yu, Q. Yao and J. Xie, *Chem. Asian J.*, 2013, 8, 858.
26. X. Yuan, Y. Tay, X. Dou, Z. Luo, T. Leong David and J. Xie, *Anal. chem.*, 2013, 85, 1913.
27. W.-Y. Chen, L.-Y. Chen, C.-M. Ou, C.-C. Huang, S.-C. Wei and H.-T. Chang, *Anal. Chem.*, 2013, 85, 8834.
28. H. Qian, D.-E. Jiang, G. Li, C. Gayathri, A. Das, R. R. Gil and R. Jin, *J. Am. Chem. Soc.*, 2012, 134, 16159.
29. H.-W. Li, Y. Yue, T.-Y. Liu, D. Li and Y. Wu, *J. Phys. Chem. C*, 2013, 117, 16159.
30. J. Liu, K. S. Krishna, Y. B. Losovyj, S. Chattopadhyay, N. Lozova, J. T. Miller, J. J. Spivey and C. S. S. R. Kumar, *Chem. Euro. J.*, 2013, 19, 10201.
31. X. Liu, F. Wang, A. Niazov-Elkan, W. Guo and I. Willner, *Nano Lett.*, 2013, 13, 309.
32. X. Liu, F. Wang, R. Aizen, O. Yehezkeli and I. Willner, *J. Am. Chem. Soc.*, 2013, 135, 11832.
33. E. S. Shibu, S. Sugino, K. Ono, H. Saito, A. Nishioka, S. Yamamura, M. Sawada, Y. Nosaka and V. Biju, *Angew. Chem. Int. Ed.*, 2013, 52, 10559.
34. B. Paramanik, S. Bhattacharyya and A. Patra, *Chem. Euro. J.*, 2013, 19, 5980.
35. J. S. Mohanty, P. L. Xavier, K. Chaudhari, M. S. Bootharaju, N. Goswami, S. K. Pal and T. Pradeep, *Nanoscale*, 2012, 4, 4255.
36. X. Dou, X. Yuan, Y. Yu, Z. Luo, Q. Yao, D. T. Leong and J. Xie, *Nanoscale*, 2014, 6, 157.
37. T. Sen, K. K. Haldar and A. Patra, *J. Phys. Chem. C*, 2010, 114, 11409.
38. T. Sen and A. Patra, *J. Phys. Chem. C*, 2012, 116, 17307.
39. D. R. Kauffman, D. Alfonso, C. Matranga, H. Qian and R. Jin, *J. Phys. Chem. C*, 2013, 117, 7914.
40. T. Udayabhaskararao, Y. Sun, N. Goswami, S. K. Pal, K. Balasubramanian and T. Pradeep, *Angew. Chem. Int. Ed.*, 2012, 51, 2155.
41. A. Murugadoss, N. Kai and H. Sakurai, *Nanoscale*, 2012, 4, 1280.
42. Z. Wu, *Angew. Chem. Int. Ed.*, 2012, 51, 2934.
43. G. Liu, D.-Q. Feng, W. Zheng, T. Chen and D. Li, *Chem. Commun.*, 2013, 49, 7941.

44. R. R. Naujok, R. V. Duevel and R. M. Corn, *Langmuir*, 1993, 9, 1771.

45. P. L. Stiles, J. A. Dieringer, N. C. Shah and R. P. Van Duyne, *Ann. Rev. Anal. Chem.*, 2008, 1, 601.

46. I. Chakraborty, S. Bag, U. Landman and T. Pradeep, *J. Phys. Chem. Lett.*, 2013, 4, 2769.

47. M. Fan, F.-J. Lai, H.-L. Chou, W.-T. Lu, B.-J. Hwang and A. G. Brolo, *Chem. Sci.* 2013, 4, 509.

Figure Captions

Scheme 1. Different pathways for synthesis of AuNC and AuAgNC.

Figure 1. (A) Absorption spectra of AuNC (a) and AuAg alloy cluster (b); (B) emission spectra of AuNC (a) and AuAg alloy cluster (b).

Figure 2. (A) Time dependent absorption spectra and (B) photoluminescence spectra of AuAg nanocluster [(a) 50 min, (b) 1h 30 min, and (c) 4h incubation time].

Figure 3. TEM images of Au nanocluster (A), AuAg bimetallic cluster (B), HAADF-STEM image of AuAg bimetallic cluster (C), elemental mapping of S (D), Au (E) and Ag (F)..

Figure 4. XPS spectra of the elements Au (A), S (B) of AuNC and (C) Au, (D) Ag of AuAg alloy nanocluster.

Figure 5. (A) Effect of different ligands on the cluster formation (a, b, c for MUA, CYS and GSH, respectively); (B) Effect of metal ions (a, b, c for Ag^+, Cu^{2+} and Pt^{4+}, respectively); (C) Stability of alloy cluster in presence of 110 mM $NaBH_4$ (a, b, and c for 0 μL, 60 μL and 120 μL and d for 120 μL of $NaBH_4$ after 1-day incubation); (D) Stability of alloy cluster in presence of 30 wt % of H_2O_2 (a, b, and c for 0 μL, 60 μL and 120 μL; d for 120 μL H_2O_2 after 10 min and e for 1-day incubation).

Figure 6. TEM images of AuNP before etching at low resolution (A), AuNP before etching at high resolution (B), after etching and before centrifugation (C), after etching and after centrifugation (D).

Figure 7. Raman spectra of pure MB (a), in presence of AuNC (b) and in presence of AuAg alloy nanocluster (c).

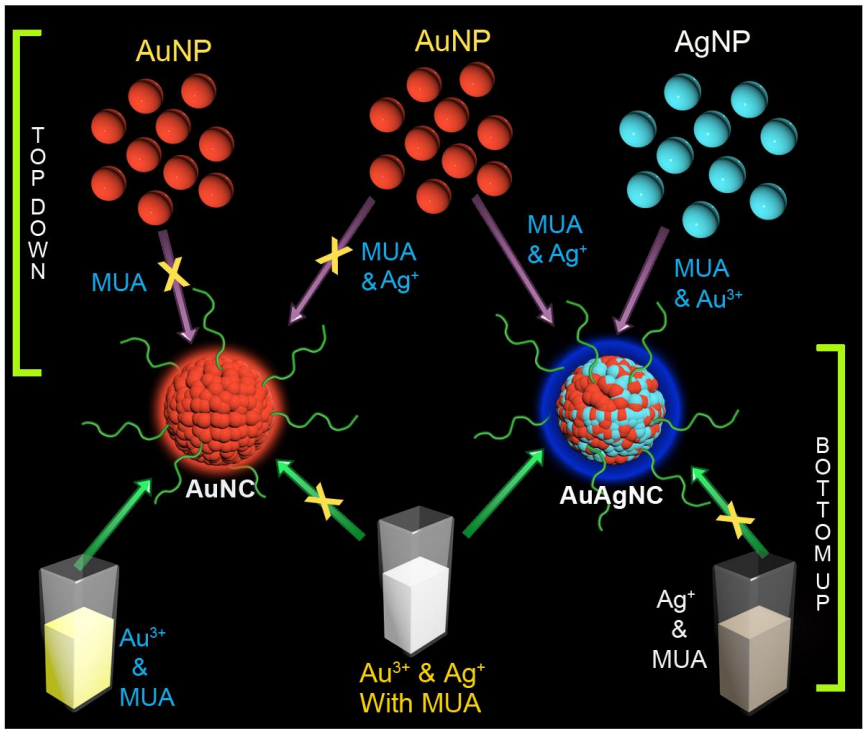

Scheme 1. Different pathways for synthesis of AuNC and AuAgNC.

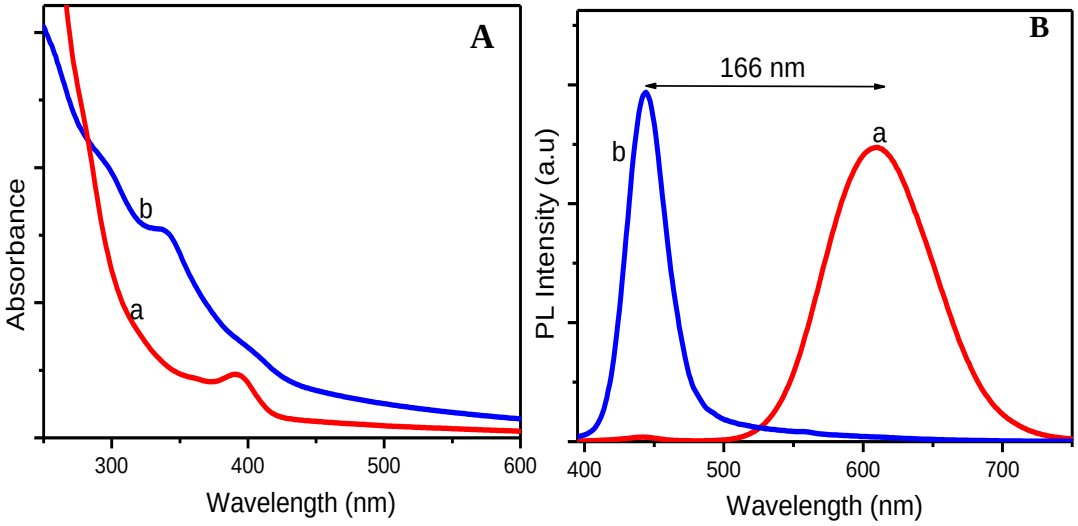

Figure 1. (A) Absorption spectra of AuNC (a) and AuAg alloy cluster (b); (B) emission spectra of AuNC (a) and AuAg alloy cluster (b).

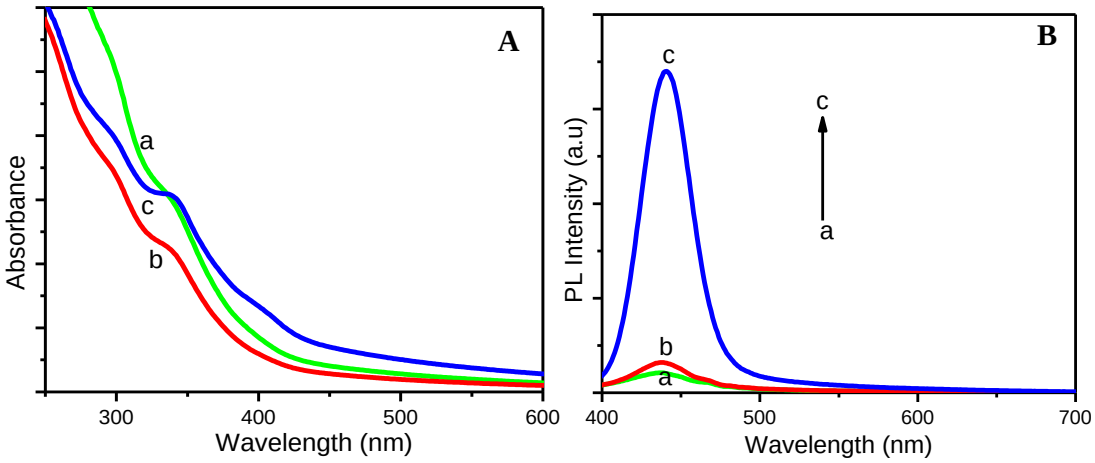

Figure 2. (A) Time dependent absorption spectra and (B) photoluminescence spectra of AuAg nanocluster [(a) 50 min, (b) 1h 30 min, and (c) 4h incubation time].

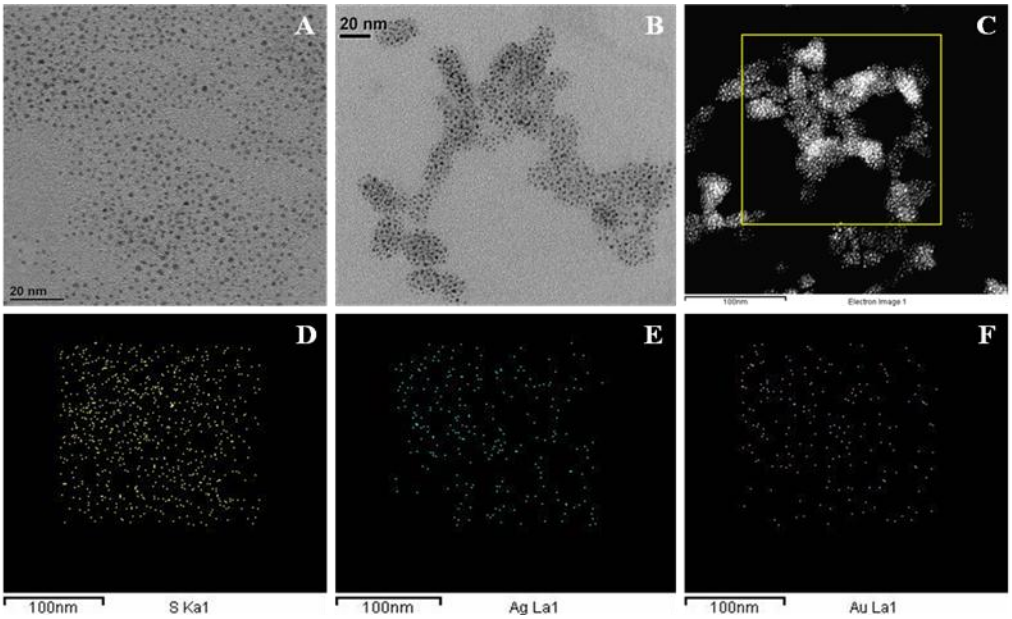

Figure 3. TEM images of Au nanocluster (A), AuAg bimetallic cluster (B), HAADF-STEM image of AuAg bimetallic cluster (C), elemental mapping of S (D), Au (E) and Ag (F).

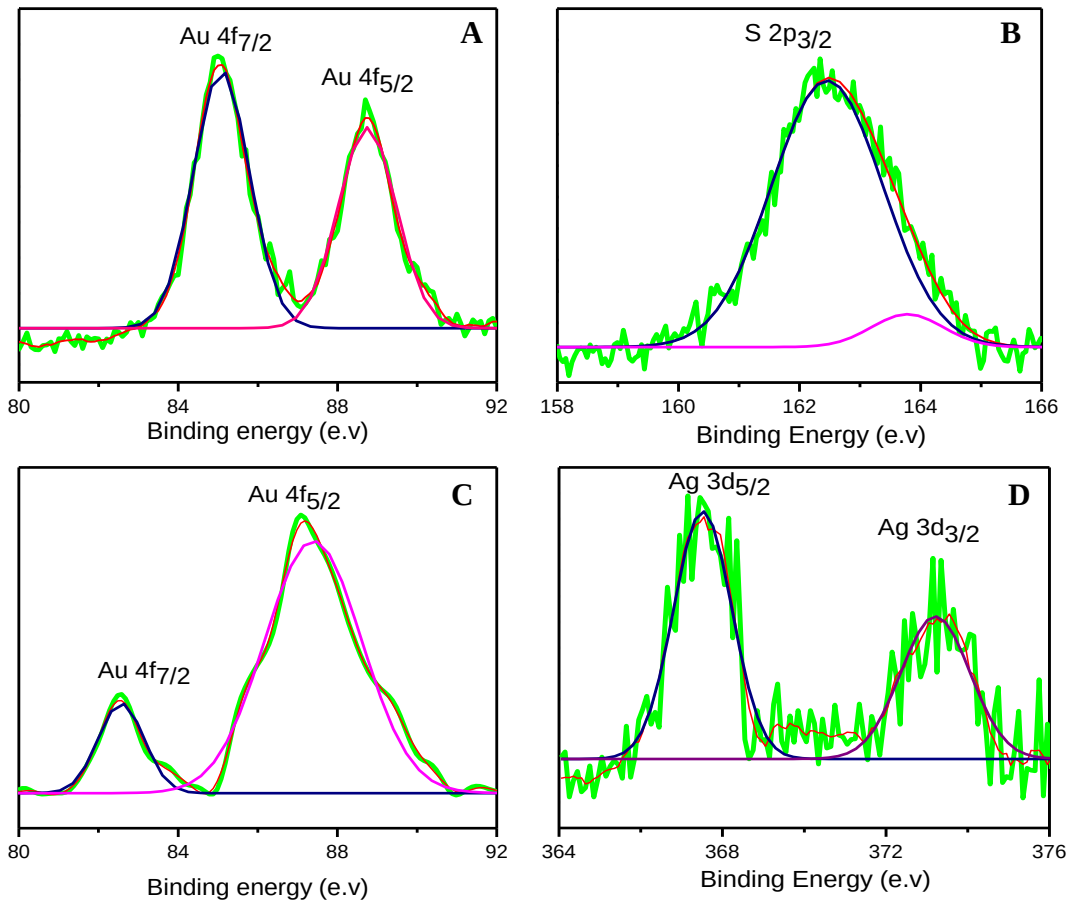

Figure 4. XPS spectra of the elements Au (A), S (B) of AuNC and (C) Au, (D) Ag of AuAg alloy nanocluster.

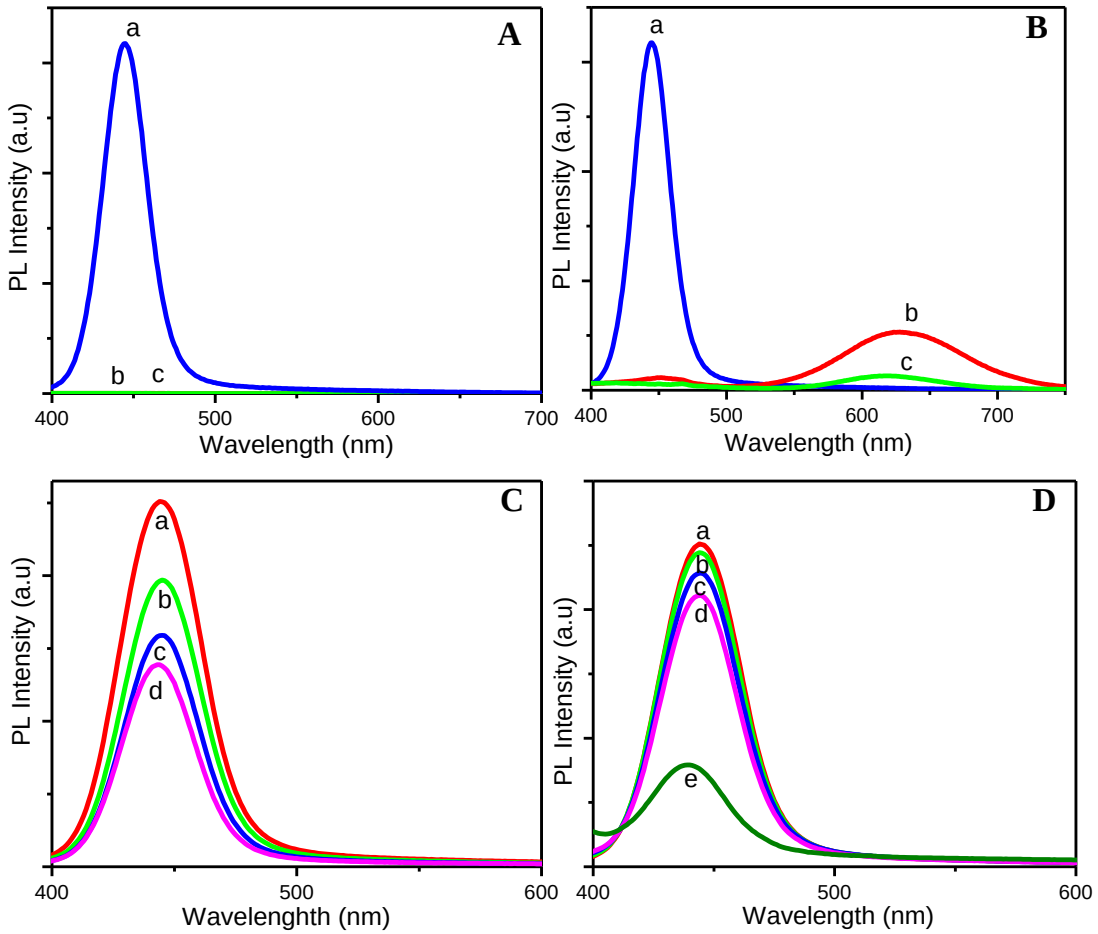

Figure 5. (A) Effect of different ligands on the cluster formation (a, b, c for MUA, CYS and GSH, respectively); (B) Effect of metal ions (a, b, c for Ag^{+}, Cu^{2+} and Pt^{4+}, respectively); (C) Stability of alloy cluster in presence of 110 mM $NaBH_4$ (a, b, and c for 0 μL, 60 μL and 120 μL and d for 120 μL of $NaBH_4$ after 1-day incubation); (D) Stability of alloy cluster in presence of 30 wt % of H_2O_2 (a, b, and c for 0 μL, 60 μL and 120 μL; d for 120 μL H_2O_2 after 10 min and e for 1-day incubation).

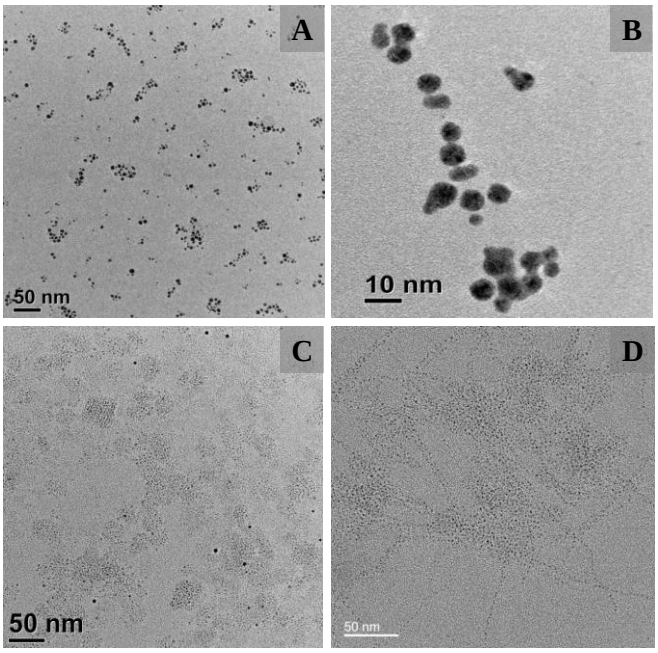

Figure 6. TEM images of AuNP before etching at low resolution (A), AuNP before etching at high resolution (B), after etching and before centrifugation (C), after etching and after centrifugation (D).

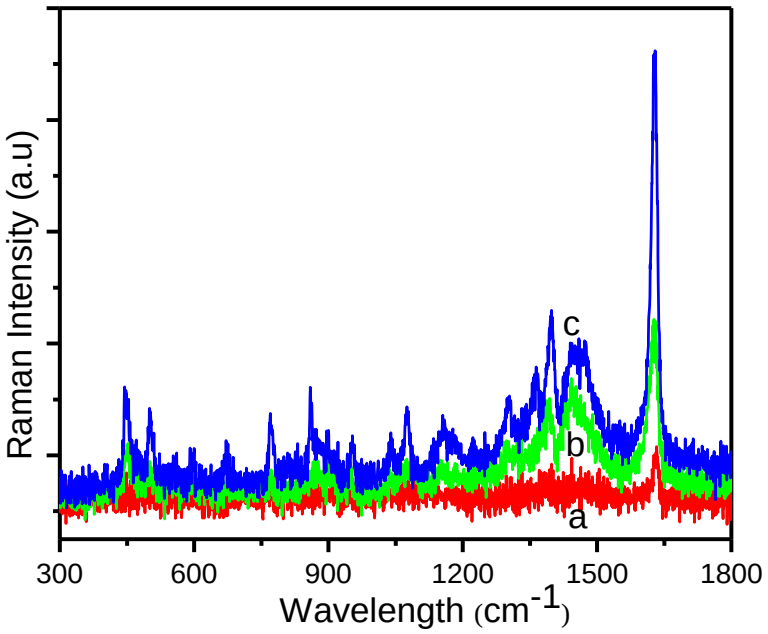

Figure 7. Raman spectra of pure MB (a), in presence of AuNC (b) and in presence of AuAg alloy nanocluster (c).

TOC: Top down and bottom up approaches for the synthesis of alloy metal clusters.